PHYSICAL REVIEW A **73**, 033405 (2006)

Alignment enhancement by the combination of a short and a long laser pulse

Mikael D. Poulsen,* Tine Ejdrup, and Henrik Stapelfeldt†
Department of Chemistry, University of Aarhus, 8000 Århus C, Denmark

Edward Hamilton and Tamar Seideman‡
Department of Chemistry, Northwestern University, 2145 Sheridan Road, Evanston, Illinois 60208-3113, USA

(Received 22 November 2005; published 2 March 2006)

The alignment dynamics of polyatomic molecules subject to two temporally overlapping nonresonant laser pulses is studied theoretically and experimentally. We examine the potential advantage of combining a long (compared to the molecular rotational periods) with a short pulse, where both laser fields are linearly polarized with common polarization direction. Experimentally, iodobenzene molecules are irradiated by a 2 ps pulse at 800 nm synchronized to the peak of a 9 ns pulse at 1064 nm. The alignment dynamics following the short laser pulse is measured using time-resolved Coulomb explosion with a delayed 25 fs-long intense laser pulse. The alignment attained with the two-pulse combination is significantly enhanced compared to that attainable with either a short or a long pulse alone under nonionizing conditions. Numerically, we solve the time dependent Schrödinger equation nonperturbatively for asymmetric top, symmetric top, and linear molecules subject to similar combinations of long and short excitation pulses. The alignment dynamics, and in particular the alignment enhancement, are explained and their generality is tested.

DOI: 10.1103/PhysRevA.73.033405 PACS number(s): 42.50.Hz, 33.80.−b, 33.15.Bh, 42.65.Re

I. INTRODUCTION

During the past decade the problem of molecular alignment by intense laser pulses has been attracting ever increasing theoretical and experimental activity due to both the interesting physics involved and the broad range of anticipated applications [1]. Two qualitatively different modes of alignment have been discussed in the literature and are relevant to the present work. The adiabatic approach [2–4] is very similar in concept and identical in mathematical structure to alignment (of nonpolar molecules) in a strong dc field. For pulses long as compared to the rotational time scale, $\tau \gg \tau_{\mathrm{rot}}$ (τ is the pulse duration, τ_{rot} the rotational period), each eigenstate of the field-free rotational Hamiltonian evolves adiabatically into the corresponding state of the complete Hamiltonian during the pulse turn-on, returning to the original (isotropic) free rotor eigenstate upon turn-off. In particular, alignment is lost after the interaction has turned off. The nonadiabatic approach [5–9] is based on general wave packet concepts. A laser pulse of short duration with respect to the rotational time scales, $\tau \ll \tau_{\mathrm{rot}}$, produces a broad superposition of rotational levels that results in alignment at a controllable time delay with respect to the pulse peak and subsequently exhibits a generic rotational revival structure. In the case of linear and symmetric top molecules the early alignment is precisely reconstructed (in the rigid rotor limit) at integer multiples of the rotational revival time. Alignment is thus available under field-free conditions. A synergy of the two approaches, where long turn-on of the laser pulse is followed by a rapid turn-off, $\tau_{\mathrm{on}} \gg \tau_{\mathrm{rot}}$, $\tau_{\mathrm{off}} \ll \tau_{\mathrm{rot}}$ has also been investigated [10,11]. In this situation the complete Hamiltonian eigenstate that has been produced in the course of the adiabatic turn-on is reconstructed subsequent to the sudden turn-off periodically in time, at multiples of the rotational revival time, and is available for applications for a controllable period under field-free conditions.

In recent years two closely related schemes of enhancing the alignment that is available through the nonadiabatic approach have been proposed and intensively investigated. The first applies two or more short pulses, appropriately time delayed with respect to one another [12–14], and the second uses optimal control theory or genetic algorithms to shape the laser field for optimizing the alignment [15–17]. Both schemes were applied also to the analog problem of short-pulse-induced orientation [18,19]. At the same time the question whether the adiabatic or nonadiabatic mode produces the sharpest alignment remains open. The possibility of applying an adiabatically turning-on, rapidly turning-off pulse [10,11] to produce the adiabatic alignment under field-free conditions makes this question relevant. What makes it nontrivial is the fact that the maximum intensity one can exert is generally determined not by the availability of sufficiently powerful laser sources but rather by the onset of competing processes. The main competing process to take into account at nonresonant frequencies is typically field ionization, as discussed in the following sections.

The main goal of the present contribution is to propose the combination of temporally overlapping long ($\tau \gg \tau_{\mathrm{rot}}$) and short ($\tau \ll \tau_{\mathrm{rot}}$) laser pulses as a means of enhancing the alignment that can be obtained from either alignment route alone under nonionizing conditions and to demonstrate its utility experimentally, theoretically, and numerically. Our motivation is twofold. First, we are intrigued by the possibility of using the combination of molecular focusing with mo-

---

*Present address: Danish Technological Institute, Kongsvang Alle 29, DK 8000 Århus C, Denmark.

†Electronic address: henriks@chem.au.dk

‡Electronic address: seideman@chem.northwestern.edu

lecular alignment to simultaneously control both the center-of-mass translation and the alignment of molecules. One application of simultaneous translational and orientational control with intense pulses, which we plan to explore experimentally and theoretically in the future, is nanoscale processing of surfaces by placing a surface at the focus of the molecular lens (see Refs. [20–22] for details). Other potential applications are noted below. As illustrated in the past, manipulation of the center-of-mass motion with intense laser pulses relies on the spatial intensity gradient of the laser beam [22–25]. Under typical molecular beam and focal spot conditions, the field-matter interaction turns on and off slowly (with respect to rotation time scales) as the molecules enter and exit the laser beam, giving rise to adiabatic alignment [10]. It is interesting to investigate the possibility of manipulating this alignment by overlapping the long molecular focusing pulse with a short pulse that produces a superposition of the eigenstates of the adiabatic Hamiltonian and hence a time-dependent alignment. From a practical perspective, the combination of a long focusing pulse with a short alignment pulse allows a certain degree of alignment to survive after the molecules have (adiabatically) excited the long-pulse laser beam and reached the focus. Our second motivation is the anticipation, based on qualitative arguments, that the combination of an adiabatic with a nonadiabatic pulse as a means of enhancing the alignment may have advantages over schemes that were previously proposed to that end for various systems of interest. This anticipation is substantiated numerically and experimentally below. Theoretically we show also that the alignment dynamics induced by the combined fields contains interesting insights into rotational coherences that could be probed in future experiments.

Before proceeding to explore the quality and controllability of the alignment produced by combined long- and short-pulse fields, it is helpful to address the related question of when a single adiabatic pulse may produce sharper alignment than a single nonadiabatic pulse. While it is clear that for fixed peak intensity a long pulse would produce sharper alignment, the question of which approach would be advantageous under conditions that avoid field ionization is nontrivial.

In the next section we briefly outline our experimental (Sec. II A) and theoretical (Sec. II B) methods. Section III presents our experimental results, focusing on the static and dynamical alignment properties of iodobenzene, an asymmetric top molecule that was studied theoretically and experimentally in previous work [26–28]. Section IV generalizes our results to other molecular symmetries and casts them in terms of transferable observables by means of theory and numerical simulations. We conclude in Sec. V with an outlook to future research.

II. METHODS

Both our theory [29] and our experimental technique [27,28] have been discussed in the recent literature and hence only brief summaries are provided here.

A. Experimental setup

A pulsed molecular beam, formed by expanding 1 mbar iodobenzene in 3 bar Helium, is crossed by three focused laser beams. One laser beam originates from a *Q*-switched Nd:YAG laser and consists of 9-ns-long almost-transform-limited pulses at 1064 nm. It is focused to a spot size $\omega_0 = 33\ \mu$m, and the highest intensity, used in the experiment, is $\sim 8 \times 10^{11}$ W/cm^2. A second laser beam consists of few-ps-long pulses (tunable from 0.1 to 4.5 ps) obtained by passing part of the output from an amplified Ti:sapphire femtosecond laser system ($\lambda = 800$ nm) through a grating stretcher. It is focused to a spot size $\omega_0 = 28\ \mu$m. The ns pulses from the Nd:YAG laser and the ps pulses from the Ti:sapphire laser are linearly polarized parallel to each other, and they are both used to align the iodobenzene molecules. The third laser beam consists of 25-fs-long pulses obtained by passing another part of the output from the Ti:sapphire system through a homebuilt hollow wave guide compressor setup [30]. The pulses have a spot size $\omega_0 = 25\ \mu$m and a peak intensity of $\sim 2 \times 10^{14}$ W/cm^2, and they are circularly polarized. These pulses are used to Coulomb explode the iodobenzene molecules in order to determine the spatial orientation of the molecular C-I axis [31].

The measurements are based on recording the direction of the I^+ ions, produced by the intense 25-fs laser pulse, because these ions recoil along the C-I axis of the parent molecule. A weak static electric field accelerates the ions towards a two-dimensional detector, and the ion images are recorded by a charge-coupled-device (CCD) camera. This enables a determination of the coordinates of each individual ion hit.

B. Theory

The complete Hamiltonian takes the form

$$H = H_{\mathrm{rot}} + \sum_{j=1,2} H_{\mathrm{ind}}^{(j)}, \tag{1}$$

where H_{ind} is the field-matter interaction and the superscript (j) distinguishes between the long $(j=1)$ and short $(j=2)$ pulses. The field-free Hamiltonian is approximated in the rigid rotor limit by the rotational kinetic energy H_{rot},

$$H_{\mathrm{rot}} = \frac{\boldsymbol{J}_X^2}{2I_{XX}} + \frac{\boldsymbol{J}_Y^2}{2I_{YY}} + \frac{\boldsymbol{J}_Z^2}{2I_{ZZ}}, \tag{2}$$

$J_k, k = X, Y, Z$ are the components of the material angular momentum vector along the body-fixed Cartesian axes, and I_{kk} are the corresponding components of the inertia tensor. The field-matter interaction in Eq. (1) is cast in the form of an induced dipole Hamiltonian [32]

$$H_{\mathrm{ind}}^{(j)} = -\frac{1}{4} \sum_{\rho,\rho'} \varepsilon_\rho^{(j)} \alpha_{\rho\rho'} \varepsilon_{\rho'}^{(j)*}, \tag{3}$$

where $\rho, \rho' = x, y, z$ are the space-fixed coordinates, α is the molecular polarizability tensor, the field is written in the semiclassical approximation as

$$\boldsymbol{\epsilon}^{(j)}(t) = \frac{1}{2}[\boldsymbol{\varepsilon}^{(j)}(t)e^{i\omega^{(j)}t} + \boldsymbol{\varepsilon}^{(j)*}(t)e^{-i\omega^{(j)}t}], \qquad (4)$$

$\boldsymbol{\varepsilon}^{(j)}(t)=\hat{\boldsymbol{\varepsilon}}\varepsilon^{(j)}(t)$, $\hat{\boldsymbol{\varepsilon}}$ is a unit vector in the field polarization direction, $\varepsilon^{(j)}(t)$ is the pulse envelope, and $\omega^{(j)}$ is the center frequency. In all calculations below the two pulses have the same temporal center, differing in the pulse duration. The long pulse is taken to have an adiabatic turn-on (long as compared to the time scale of rotation about the largest moment of inertia) and hereafter it remains constant at the peak intensity value. The short pulse is Gaussian with the duration of the experimental pulse.

Restricting attention to the case of linearly polarized fields and transforming the polarizability tensor from the space-to the body-fixed frame (see Ref. [33], Table 1) we have

$$H_{\mathrm{ind}}^{(j)} = -\frac{1}{4}[\varepsilon^{(j)}(t)]^2[\alpha^{ZX}\cos^2\theta + \alpha^{YX}\sin^2\theta\sin^2\chi], \qquad (5)$$

where we introduced generalized polarizability anisotropies as $\alpha^{ZX}=\alpha_{ZZ}-\alpha_{XX}$, $\alpha^{YX}=\alpha_{YY}-\alpha_{XX}$, α_{kk}, $k=X,Y,Z$, are the body-fixed components of the polarizability tensor, and $\hat{R}=(\theta,\phi,\chi)$ are the Euler angles of rotation specifying the orientation of the body-with respect to the space-fixed frame. In Eq. (5) we omit a term independent of the angles that amounts to an overall shift of the potential and has no effect on the alignment dynamics.

The time evolution during and after the short laser pulse is determined nonperturbatively by expanding the wave packet in a complete set of stationary eigenstates, to convert the time-dependent Schrödinger equation into a set of first-order coupled differential equations. To maximize the efficiency of the solution, we use a basis set of symmetric top eigenstates during the pulse and a basis of eigenstates of the field-free Hamiltonian after the turn-off of the short pulse. A transformation between the symmetric top and asymmetric top basis sets is applied in calculations dealing with asymmetric top molecules. The associated transformation matrix is sparse, making this a numerically inexpensive operation. The alternative of computing the eigenstates of the adiabatic Hamiltonian, $H_{\mathrm{rot}}+H_{\mathrm{ind}}^{(1)}(t=t_0)$ (where t_0 is the temporal center of the pulses), and expanding the wave packet as a superposition of these eigenstates before and after the short pulse is conceptually appealing but numerically difficult, since the calculated observables are more easily computed in the symmetric top basis and the transformation between the adiabatic states and the free rotor symmetric top states involves a dense transformation matrix.

With the time-dependent wave packet $\Psi_i(t)$ corresponding to a set of initial conditions collectively denoted by i determined, all observables can be computed nonperturbatively as a function of time. The expectation value of $\cos^2\theta$ in the wave packet, $\langle\cos^2\theta\rangle_i(t)=\langle\Psi_i|\cos^2\theta|\Psi_i\rangle$, is the observable most commonly used for quantification of the alignment and is also used here. We remark, however, that it does not provide all the information available in the probability density (as it is conveys the second moment of the alignment alone) and that its maximum may be slightly shifted with respect to the alignment maximum of the wave packet probability density. The thermal analog $\langle\cos^2\theta\rangle_T(t)$ is obtained through Boltzmann averaging of the $\langle\cos^2\theta\rangle_i(t)$ at a rotational temperature T. More details of our theory and numerical implementation are provided in Ref. [29].

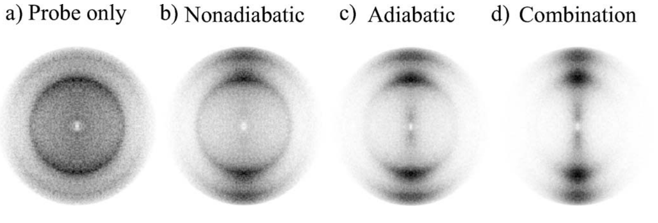

FIG. 1. Images of the I^+ ions originating from Coulomb explosion of iodobenzene at different alignment pulse conditions. (a) Probe only. (b) Strongest alignment obtained with a 2.1-ps-long pulse ($I_0=6\times10^{12}$ W/cm^2). (c) The alignment obtained with a 9-ns-long pulse ($I_0=8\times10^{11}$ W/cm^2). (d) Strongest alignment with both the 2.1-ps pulse ($I_0=6\times10^{12}$ W/cm^2) and the 10-ns pulse ($I_0=8\times10^{11}$ W/cm^2). The probe pulse is circularly polarized and the two alignment pulses are linearly polarized along the vertical axis.

III. EXPERIMENTAL RESULTS

In Fig. 1(a) we show an I^+ ion image recorded when only the intense 25-fs probe pulse is incident on the iodobenzene molecules. The radial structure in the image originates from multiphoton ionization of C_6H_5I and subsequent Coulomb fragmentation [31]. The spatial orientation of the molecules is quantified by the average value of $\cos^2\theta_{2d}$, $\langle\cos^2\theta_{2d}\rangle$, where θ_{2d} is the angle between the projection of the I^+ velocity vector (the orientation of the C-I bond) and the polarization direction of the alignment pulses (vertical in the images). The I^+ ions in the outer half rings are produced from triple ionization of C_6H_5I and Coulomb explosion into I^+ and $C_6H_5^{2+}$ [31]. Using a radial range that includes only the outer ring a $\langle\cos^2\theta_{2d}\rangle$ value of 0.65 is obtained when the probe pulse alone is used. The deviation from circular symmetry ($\langle\cos^2\theta_{2d}\rangle=0.50$) is due to the angular selectivity of the probe ionization process. Molecular alignment, expected when the alignment pulses are included, should manifest itself as an increase in the value of $\langle\cos^2\theta_{2d}\rangle$ corresponding to an angular narrowing of the ion image in Fig. 1(a).

In the first part of our experiment we measured the alignment induced by either the long (YAG) pulse or the short (800-nm) pulse. In each case the laser parameters were adjusted to optimize the degree of alignment. For adiabatic alignment, created by the YAG pulse, the intensity is the only parameter that determines the degree of alignment (for a fixed rotational temperature of the molecular sample). The results, displayed in Fig. 2, show that the degree of alignment increases monotonically with intensity in accordance with previous measurements [31,34]. For experimental reasons the highest YAG intensity used was 8×10^{11} W/cm^2 but the degree of alignment can be slightly enhanced by increasing the YAG intensity to a few times 10^{12} W/cm^2 which is where ionization starts to occur [31].

For nonadiabatic alignment, created by the 800-nm pulse, the degree of alignment is determined by the intensity, the

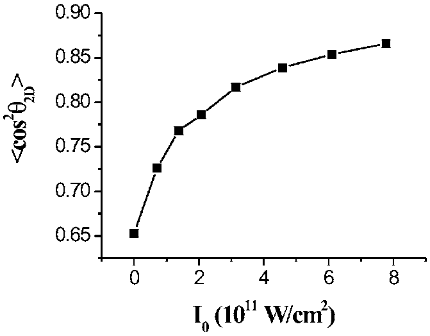

FIG. 2. Intensity dependence of the adiabatic alignment obtained by the long (YAG) pulse alone. The $\langle\cos^2\theta_{2d}\rangle$ values are determined from the outer half rings of the I^+ images. The lines between the points serve to guide the eye.

pulse duration,[1] and the time relative to the pulse. To find the parameters for which the strongest alignment occurs the alignment dynamics after the pulse was measured for four different pulse durations. We only measure the alignment dynamics at early times after the pulse because the global maximum occurs here rather than at any of the subsequent revivals [27]. In each case the intensity was tuned just below the value where ionization starts to occur. The results displayed in Fig. 3 show that the degree of alignment reaches a maximum immediately after the pulse whereupon it decreases rapidly. The alignment dynamics corresponds to an initial constructive interference of the components in the rotational wave packet and subsequent dephasing as detailed previously [10,27]. The strongest alignment is approximately the same at the four different durations with the $\langle\cos^2\theta_{2d}\rangle$ values located in the range 0.805–0.815. For the 1.1 ps, 1.5 ps, and 3.1 ps pulse durations the alignment maximum occurs while the pulse is still on whereas for the 2.1 ps duration the alignment maximum occurs after the pulse is turned off—i.e., under field-free conditions. We note that the maximum degree of alignment achieved in the adiabatic regime is significantly higher than the maximum degree of alignment in the nonadiabatic regime. This is also evident by comparing the ion images in Figs. 1(c) and 1(b) obtained with the YAG pulse at $I_0=8\times10^{11}$ W/cm^2 and for the 2.1-ps-long 800-nm pulse at time 2.7 ps, respectively.

In the second part of our experiment we measured the alignment resulting from exposing the molecules to both the long (YAG) pulse and the short (800-nm) pulse. The alignment dynamics following the 800-nm pulse is displayed in Fig. 4 for three different combinations of the YAG and 800-nm pulse intensities. The pulse duration of the 800-nm pulse was fixed at 2.1 ps. In all cases the alignment reaches a maximum 1–2 ps after the center of the 800-nm pulse. The alignment at the maximum is significantly stronger than the best alignment reached by any of the two pulses alone. This is also clear from comparing the tightly angularly confined image in Fig. 1(d) to the images in Fig. 1(b) or 1(c).

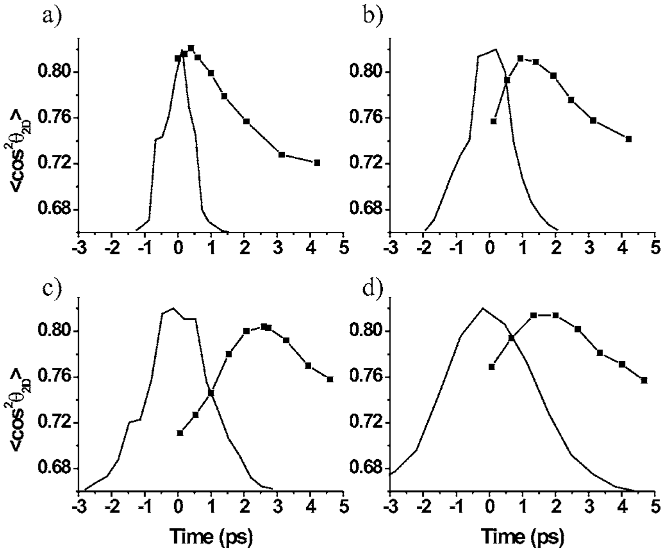

FIG. 3. Nonadiabatic alignment of iodobenzene, quantified by $\langle\cos^2\theta_{2d}\rangle$, induced by pulses with different durations. (a) $\tau_{FWHM}=1.1$ ps, $I_0=6.9\times10^{12}$ W/cm^2, (b) $\tau_{FWHM}=1.5$ ps, $I_0=6.2\times10^{12}$ W/cm^2, (c) $\tau_{FWHM}=2.1$ ps, $I_0=5.8\times10^{12}$ W/cm^2, and (d) $\tau_{FWHM}=3.1$ ps, $I_0=4.9\times10^{12}$ W/cm^2. The lines between the points serve to guide the eyes. In each subfigure the solid curve shows the intensity envelope of the alignment pulse. Without an alignment pulse $\langle\cos^2\theta_{2d}\rangle=0.65$.

After reaching a maximum $\langle\cos^2\theta_{2d}\rangle$ drops below the value resulting from the YAG pulse alone (indicated by the horizontal lines in the three subfigures) and reaches a minimum at a time depending on the intensity of the two pulses. The minimum occurs at ~15 ps, ~6.5 ps, and ~5.5 ps for Figs. 4(a)–4(c), respectively. Following the minimum the degree of alignment recovers but stays below the adiabatic value. At the highest intensity of the YAG pulse and 800-nm pulse the experimental data indicate an oscillatory behavior in $\langle\cos^2\theta_{2d}\rangle$ [Fig. 4(c)].

IV. NUMERICAL RESULTS

In this section we explore the origin of the observations of Sec. III, and the extent to which they are general, by numerical calculations and theoretical analysis. In Fig. 5 we consider the alignment dynamics of iodobenzene subject to a combination of a long and a short pulse (solid curves) and compare these to the cases of a single short pulse (dashed curves) and a single long pulse (dotted curve). The short pulse duration is as in the experimental study and the intensities of the long and short pulses are chosen slightly below the field ionization limit, as in the experiment illustrated in Fig. 4.

We stress that a quantitative comparison of the experimental and numerical results is not sought. For several reasons such a comparison is not possible at the present stage. First the rotational temperature in the experiment is not known. The accuracy to which the intensity can be experimentally determined is likewise limited. Further, in our present experiments the probe samples much of the focal volume of the alignment laser. Consequently the intensity is not uniform and it is necessary to average calculations per-

---

[1] More precisely, the turn-on and turn-off times; see Ref. [10].

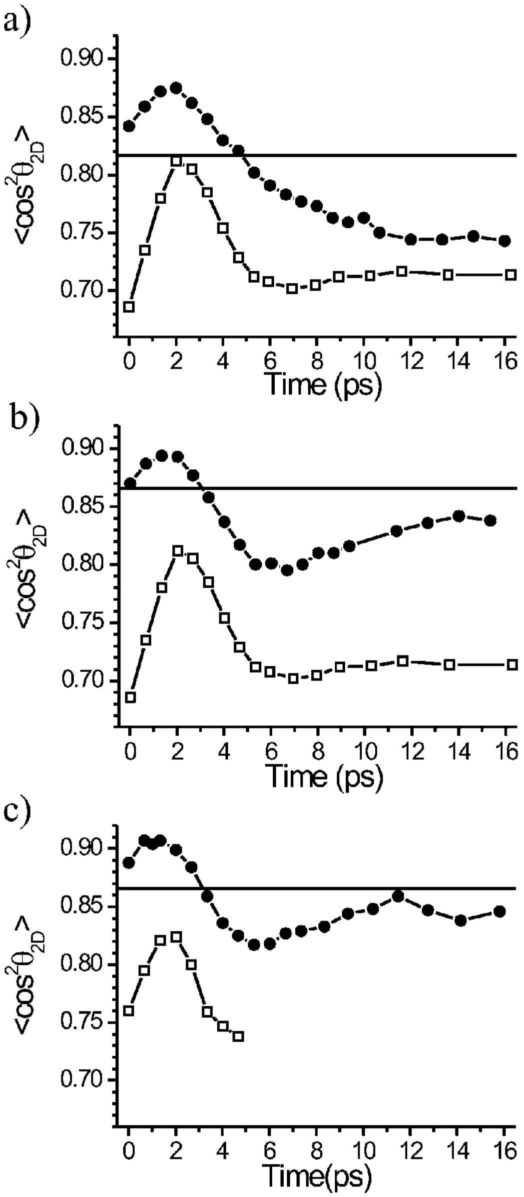

FIG. 4. $\langle \cos^2 \theta_{2D} \rangle$ determined from ion images of iodobenzene subject to a 2.1-ps nonadiabatic pulse centered at $t=0$ (squares), an adiabatic alignment pulse (solid line), or both pulses (circles). Lines between points serve to guide the eye. The peak intensities were (a) $I_0(\text{nonadiabatic}) = 3.5 \times 10^{12}$ W/cm^2, $I_0(\text{adiabatic}) = 3.1 \times 10^{11}$ W/cm^2, (b) $I_0(\text{nonadiabatic}) = 3.5 \times 10^{12}$ W/cm^2, $I_0(\text{adiabatic}) = 7.8 \times 10^{11}$ W/cm^2, and (c) $I_0(\text{nonadiabatic}) = 5.8 \times 10^{12}$ W/cm^2, $I_0(\text{adiabatic}) = 7.8 \times 10^{11}$ W/cm^2.

formed at different intensities with proper weight functions in order to contrast numerical and experimental results, a procedure that washes out several of the features that are observed in single intensity calculations [28]. To be reliably performed, the focal averaging requires experimental determination of not only the peak, but also the spatial distribution of the intensity. In addition, numerically we compute the alignment dynamics (using $\langle \cos^2 \theta \rangle$ as an average measure) whereas our experimental observable $\langle \cos^2 \theta_{2d} \rangle$ reflects also the detection dynamics.

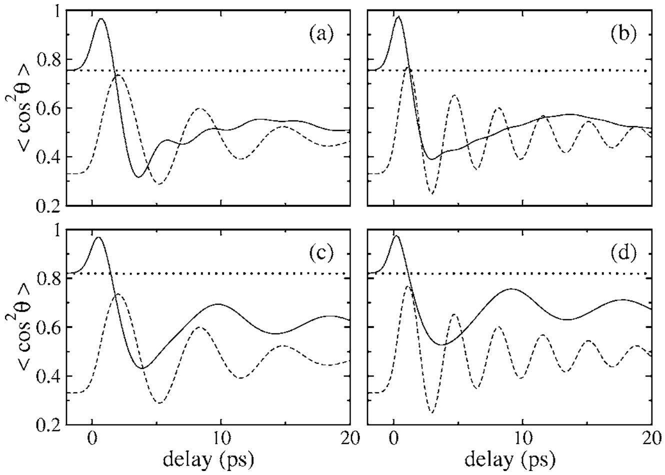

FIG. 5. Computed alignment dynamics of iodobenzene at 400 mK subject to an adiabatic (long) pulse (dotted curves), a nonadiabatic (short) pulse (dashed curves), and a combination of both pulses (solid curves). The duration of the nonadiabatic pulse is 2.1 ps. (a) $I_0(\text{adiabatic}) = 3 \times 10^{11}$ W/cm^2, $I_0(\text{nonadiabatic}) = 3 \times 10^{12}$ W/cm^2; (b) $I_0(\text{adiabatic}) = 3 \times 10^{11}$ W/cm^2, $I_0(\text{nonadiabatic}) = 6 \times 10^{12}$ W/cm^2; (c) $I_0(\text{adiabatic}) = 6 \times 10^{11}$ W/cm^2, $I_0(\text{nonadiabatic}) = 3 \times 10^{12}$ W/cm^2; and (d) $I_0(\text{adiabatic}) = 6 \times 10^{11}$ W/cm^2, $I_0(\text{nonadiabatic}) = 6 \times 10^{12}$ W/cm^2.

The qualitative conclusions of Sec. III are clearly supported by the numerical results of Fig. 5. In particular, whereas the peak alignment produced by the separate adiabatic and short pulses is comparable (for the set of conditions considered), the combination of the long and short pulses produces significantly sharper alignment. More careful inspection of Fig. 5 illustrates that the alignment subject to the combined fields is unprecedented, while the parameters of the field, based on our experiments, are realistic. It is important to stress, however, that the temperature in Fig. 5 is relatively low, corresponding to a Boltzmann average of angular momentum states $J_i = 0-7$, $-J_i \leqslant M_i \leqslant J_i$ in the parent state. The degree of alignment degrades rapidly with increasing rotational temperature. (This applies to the isolated molecule limit. In dissipative media the role of temperature is more complex [35].) Other features of Fig. 5 are similarly in good agreement with the experimental results of Fig. 4. Subsequent to the initial sharp peak, where $\langle \cos^2 \theta \rangle$ rises well above the adiabatic limit, the alignment drops and exhibits a broad structure. This structure reflects the beating of several eigenstates of the adiabatic pulse Hamiltonian (the stationary Hamiltonian that includes the rotational Hamiltonian and the adiabatic pulse at its peak value, often termed "pendular Hamiltonian" in the case of linear molecules [2]) that are excited by the short pulse, and its details depend on the intensities of both pulses, as elaborated below. At the intensity regime of Figs. 4 and 5, the alignment induced by the combined fields is higher than that available from the nonadiabatic excitation alone and is less structured, since a given short pulse can excite a much broader superposition of field-free rotor states in the absence of the adiabatic pulse than the superposition of dressed states the same pulse can excite in the presence of the long pulse. The results of Figs. 4 and 5 have been anticipated. Since the short pulse produces a su-

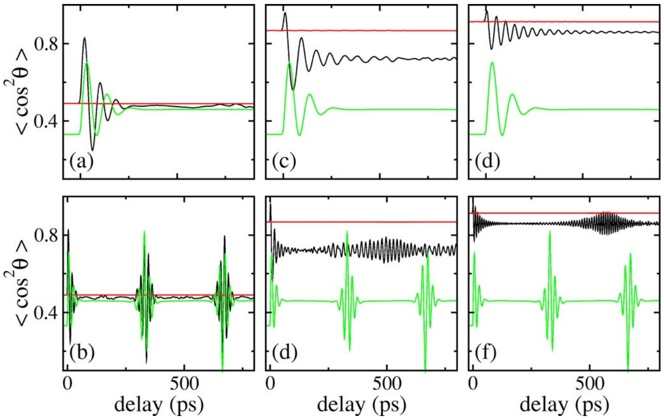

FIG. 6. (Color online) Computed alignment dynamics of a model symmetric top subject to a long adiabatic pulse (red), a sudden pulse (green), and the combination of long and short pulses (black). The rotational constants are chosen so as to keep the relative system and field time scales as close as possible to those of the iodobenzene experiment ($C_e = B_e = 0.748$ GHz, $A_e = 5.68$ GHz) while exploring a different symmetry. The polarizability components are chosen so as to keep the relative strength of the molecular and field-matter Hamiltonians as close as possible to those of the iodobenzene experiment ($\alpha_{XX} = \alpha_{YY} = 105.3$, $\alpha_{ZZ} = 152.6$ bohr^3). The duration of the short pulse is as in Figs. 4 and 5. In panels (a) and (b) the intensity of the long pulse is 1×10^{10} W/cm^2 and that of the nonadiabatic pulse is 6×10^{11} W/cm^2. In panels (c) and (d) the intensity of the adiabatic pulse is increased by a factor of 20 and in panels (e) and (f) by a factor of 50 as compared to panels (a), and (b). Panels (a), (c), and (e) show the short-time, and panels (b), (d), and (f) the long-time alignment dynamics.

perposition of the eigenstates of the adiabatic pulse Hamiltonian, the resulting beat pattern is expected to transiently exceed the stationary value of $\langle \cos^2 \theta \rangle$ established by the long pulse.

In order to explore the generality of these results, we have repeated the calculation for a symmetric top and linear rotor. To keep constant the relative system and field time scales and the relative free Hamiltonian and interaction Hamiltonian strengths, we consider artificial model molecules whose polarizability and inertia tensors have the symmetric top and linear rotor symmetries but are otherwise identical to those of the iodobenzene system studied in our experiments. Comparison of Fig. 5 with panel (c) of Fig. 6 illustrates that the message of Figs. 4 and 5 applies equally to symmetric top systems. The same result has been obtained for the linear case.

Both the experimental and numerical results show that the alignment peak in the case of combined fields appears earlier than the alignment peak in the case of the nonadiabatic pulse alone. Consequently, the alignment peak in the case of combined fields occurs when both fields are on under the conditions of Figs. 4 and 5. This raises the concern that the revival pattern produced by the short pulse—the recurrence structure of the wave packet of the adiabatic Hamiltonian eigenstates—would correspond to a much less sharp alignment than the early peak value. This expectation is borne by the long-time calculations illustrated in Fig. 6(d), where we retain the pulse duration and intensities of the combined-fields experiment but explore the alignment evolution at much longer times than those probed by our experiment. Whereas the initial combined-fields alignment rises well above the adiabatic alignment limit, the subsequent revival peaks fall short. The details of the revival structures of Figs. 6(b), 6(d), and 6(f) are discussed at the end of the section.

An interesting and practically pertinent question is thus if, and under what conditions, the combined-fields effect could produce long-time revival features that exceed the adiabatic limit. Theoretical considerations, based on an analytical solution of the linear molecule case, suggest that both at lower intensities of the adiabatic field, below the range used in our experiments, and at higher adiabatic field intensities than those used in our experiments the combined fields provide a long-time advantage over the adiabatic route alone. Panels (b) and (f) of Fig. 6 support this suggestion numerically. The case of a low adiabatic field intensity is studied in Figs. 6(a) and 6(b), whereas the case of high adiabatic field intensity is studied in Figs. 6(e) and 6(f).

We note in Figs. 6(b), 6(d), and 6(f) the gradual change of the revival structure from that typical of rotational revivals to that characterizing a *librational* wave packet as the intensity of the adiabatic pulse increases. For relatively low interaction strength of the long pulse, $\Omega_R = (\varepsilon^{(1)})^2(\alpha_{ZZ} - \alpha_{XX})$ comparable to the rotational energy [Fig. 6(a)], the long-time alignment dynamics resulting from the combined fields resembles that corresponding to the short pulse alone. The latter is a characteristic revival pattern of symmetric top molecules, shown in Ref. [29] to have common features with the extensively studied case of rotational revivals from linear molecules, but exhibit an additional structure, corresponding to rotation about two axes. As the intensity of the long pulse grows, adiabatic alignment subject to the gradual turn-on of the long pulse produces eigenstates of the adiabatic Hamiltonian $H_{\text{rot}} + H_{\text{ind}}^{(1)}$ that consist of broader superpositions of free rotor states and are better spatially aligned, corresponding, in rough language, to librational, rather than free rotational motion. The alignment dynamics subsequent to turn-off of the short pulse exhibits the revival pattern of a librational wave packet—a superposition of the $H_{\text{rot}} + H_{\text{ind}}^{(1)}$ eigenstates that is coherently excited by the short pulse. The time scales in Figs. 6(d) and 6(f) are thus a direct measure of the librational motion of the molecule in the $\cos^2 \theta$-shaped potential well produced by the long pulse. The rapid oscillations correspond to the period of the librational dynamics. This period, as expected, decreases as the intensity of the adiabatic pulse is increased and the gradient of the laser-induced potential at the equilibrium configurations $\theta = 0$ is increased. The envelope of the oscillation observed in Fig. 6(f) corresponds to the revival pattern of the librational wave packet. Its time scale increases as the intensity is increased, as the anharmonicity of the librational motion decreases.

V. CONCLUSIONS

The previous sections have studied the alignment dynamics of polyatomic molecules interacting simultaneously with a long (compared to the rotational periods) and a short (compared to the rotational periods) laser pulse. To that end we combined a nonperturbative solution of the time-dependent Schrödinger equation with time-resolved photofragment imaging technology. One of our goals in this research has been to explore the possibility of combining molecular alignment with the related technique of molecular optics, wherein the spatial intensity gradient of the laser beam is used to manipulate the center-of-mass motion of molecules. A second motivation has been the current worldwide effort to introduce methods of optimizing the nonadiabatic alignment and three-dimensional (3D) alignment of molecules. Experimentally, we measured the alignment characteristics of iodobenzene subject to a single adiabatic pulse, a single short pulse, and the combination of both pulses for different field parameters. Numerically we first applied these three alignment approaches to iodobenzene, keeping the relative system and field time scales and the relative strengths of the field-free and interaction Hamiltonians as in the experiment. We then repeated the calculation for different molecular symmetries and for different relative strengths of the molecular and interaction Hamiltonians. Our numerical results support the conclusions of our measurements and generalize them to classes of molecules different from the one probed. They also point to a trade-off between the desired alignment characteristics that is controlled by the parameters of the two pulses. Finally, a numerical study of the long-time evolution illustrated the revival pattern of a librational wave packet, corresponding to the beat pattern of a wave packet of eigenstates of the adiabatic Hamiltonian. One of our goals in ongoing experimental and theoretical research is to extend these results to the case where the long- and short-pulse electric fields are not parallel to one another (and may or may not be orthogonal), and hence their combined effect produces 3D alignment.

ACKNOWLEDGMENTS

T.S. is grateful to the U.S. Department of Energy (Grant No. DE-FG02-04ER15612) for support of this research. H.S. is grateful to the Carlsberg Foundation, The Lundbeck Foundation, and the Danish Natural Science Research Council for support. We acknowledge the excellent support of Jan Thøgersen and the technical staff members at the Departments of Chemistry and Physics, University of Aarhus.

---

[1] H. Stapelfeldt and T. Seideman, Rev. Mod. Phys. **75**, 543 (2003).
[2] B. Friedrich and D. Herschbach, Phys. Rev. Lett. **74**, 4623 (1995).
[3] W. Kim and P. Felker, J. Chem. Phys. **104**, 1147 (1996).
[4] H. Sakai, C. P. Safvan, J. J. Larsen, K. M. Hilligsøe, K. Hald, and H. Stapelfeldt, J. Chem. Phys. **110**, 10235 (1999).
[5] T. Seideman, J. Chem. Phys. **103**, 7887 (1995).
[6] J. Ortigoso, M. Rodríguez, M. Gupta, and B. Friedrich, J. Chem. Phys. **110**, 3870 (1999).
[7] C. M. Dion, A. Keller, O. Atabek, and A. D. Bandrauk, Phys. Rev. A **59**, 1382 (1999).
[8] T. Seideman, Phys. Rev. Lett. **83**, 4971 (1999).
[9] F. Rosca-Pruna and M. J. J. Vrakking, Phys. Rev. Lett. **87**, 153902 (2001).
[10] T. Seideman, J. Chem. Phys. **115**, 5965 (2001).
[11] J. G. Underwood, M. Spanner, M. Yu Ivanov, J. Mottershead, B. J. Sussman, and A. Stolow, Phys. Rev. Lett. **90**, 223001 (2003).
[12] M. Leibscher, I. Sh. Averbukh, and H. Rabitz, Phys. Rev. A **69**, 013402 (2004).
[13] K. F. Lee, I. V. Litvinyuk, P. W. Dooley, M. Spanner, D. M. Villeneuve, and P. B. Corkum, J. Phys. B **37**, L43 (2004).
[14] C. Z. Bisgaard, M. D. Poulsen, E. Péronne, S. S. Viftrup, and H. Stapelfeldt, Phys. Rev. Lett. **92**, 173004 (2004).
[15] K. Hoki and Y. Fujimura, Chem. Phys. **267**, 267 (2001).
[16] M. Renard, E. Hertz, B. Lavorel, and O. Faucher, Phys. Rev. A **69**, 043401 (2004).
[17] D. Sugny, A. Keller, O. Atabek, D. Daems, C. M. Dion, S. Guerin, and H. R. Jauslin, Phys. Rev. A **71**, 063402 (2004).
[18] C. M. Dion, A. Ben Haj-Yedder, E. Cances, C. Le Bris, A. Keller, and O. Atabek, Phys. Rev. A **65**, 063408 (2002).
[19] D. Sugny, A. Keller, O. Atabek, D. Daems, C. M. Dion, S. Guerin, and H. R. Jauslin, Phys. Rev. A **69**, 033402 (2005).
[20] T. Seideman, Phys. Rev. A **56**, R17 (1997).
[21] T. Seideman, J. Chem. Phys. **106**, 2881 (1997).
[22] R. J. Gordon, L. Zhu, W. A. Schroeder, and T. Seideman, J. Appl. Phys. **94**, 669 (2003).
[23] H. Stapelfeldt, H. Sakai, E. Constant, and P. B. Corkum, Phys. Rev. Lett. **79**, 2787 (1997).
[24] B. S. Zhao, S. H. Lee, H. S. Chung, S. Hwang, W. K. Kang, B. Friedrich, and D. S. Chung, J. Chem. Phys. **119**, 8905 (2003).
[25] R. Fulton, A. I. Bishop, and P. F. Barker, Phys. Rev. Lett. **93**, 243004 (2004).
[26] E. Péronne, M. D. Poulsen, C. Z. Bisgaard, H. Stapelfeldt, and T. Seideman, Phys. Rev. Lett. **91**, 043003 (2003).
[27] M. D. Poulsen, E. Péronne, H. Stapelfeldt, C. Z. Bisgaard, S. S. Viftrup, E. Hamilton, and T. Seideman, J. Chem. Phys. **121**, 783 (2004).
[28] E. Péronne, M. D. Poulsen, H. Stapelfeldt, C. Z. Bisgaard, E. Hamilton, and T. Seideman, Phys. Rev. A **70**, 063410 (2004).
[29] E. Hamilton, T. Seideman, T. Ejdrup, M. D. Poulsen, C. Z. Bisgaard, S. S. Viftrup, and H. Stapelfeldt, Phys. Rev. A **72**, 043402 (2005).
[30] J. Olesen, Master's thesis, Department of Chemistry, University of Aarhus, 1999.
[31] J. J. Larsen, H. Sakai, C. P. Safvan, I. Wendt-Larsen, and H. Stapelfeldt, J. Chem. Phys. **111**, 7774 (1999).
[32] T. Seideman, J. Chem. Phys. **111**, 4397 (1999).
[33] T. Seideman, Chem. Phys. Lett. **253**, 279 (1996).
[34] M. D. Poulsen, E. Skovsen, and H. Stapelfeldt, J. Chem. Phys. **117**, 2097 (2002).
[35] S. Ramakrishna and T. Seideman, Phys. Rev. Lett. **95**, 113001 (2005).